Photocontrollable Phase Separation in Two-Dimensional Molecular Films

Takashi Ubukata,[†] Kunihiro Ichimura,[‡] and Takahiro Seki*[,§]

Local Spatio-Temporal Functions Laboratory, Frontier Research System, RIKEN, 2-1 Hirosawa, Wako, Saitama 351-0198, Japan, Research Institute for Science and Technology, Tokyo University of Science, 2641 Yamazaki, Noda, Chiba 278-8510, Japan, and Department of Applied Chemistry, Nagoya University, Chikusa, Nagoya, Aichi 464-8603, Japan

Received: May 8, 2003; In Final Form: October 17, 2003

Two-dimensional (2D) molecular films composed of mixtures of an amphiphilic polymer containing an azobenzene (Az) side chain [6Az10-PVA; PVA = poly(vinyl alcohol)] and a nematic liquid crystal molecule, 4′-pentyl-4-cyanobiphenyl (5CB), are prepared on both the water surface and solid substrate at various molar ratios. The compatibility and phase separation behavior of the two components in two dimensions are examined. Surface pressure area isotherms and atomic force microscopy shows that 2D phase separation starts to occur on a submicrometer scale above the critical ratio of 5CB to Az units ($r = 2$), while the two components are homogeneously mixed at a molecular level and form a hybrid monolayer up to the critical ratio. It is further revealed that phase separation is composed of projecting thicker domains of the 6Az10-PVA/5CB molecular hybrid ([Az]/[5CB] = 1:2) and pure 5CB continuous phase. Photochemical reversible control of phase separation is visualized for the first time with alternating irradiation of UV and visible light.

1. Introduction

In the field of optoelectronic devices, controlled and tunable preparation of submicrometer- and micrometer-sized structures in materials, by physical or chemical methods, has become an important branch of advanced materials in recent years. One example is the so-called polymer-dispersed liquid crystals (PDLCs).[1−4]

The PDLC films are promising new optoelectronic materials being developed for use in thin flexible flat-panel displays and windows. Although there are many kinds of PDLCs,[5−8] basically they are composed of micrometer-sized droplets of liquid crystal (LC) dispersed in a polymer matrix. The PDLC films are switched between a light-scattering state and a transparent one depending on the orientation of the LC molecules. The mismatching and matching of the refractive indices of the LC and the polymer make this effect. Light scattering and transmitting properties depend on the optical properties of polymer and LC, droplet size, and shape.

On the other hand, much attention has been paid to photonics, in which light can be controlled by other light, as a future technology for high-speed information processing.[9] The amount of information dealt with in our society is growing so large that faster information transfer is essential. Light has outstanding characteristic properties such as intensity, polarization, and wavelength. These properties are particularly useful in information processing. Photoswitchable PDLC films have also been proposed quite recently.[10−13] They are coupled with photochemically induced phase-transition phenomena of LCs to obtain reversible, rapid, and long-lasting photorecording devices. In these systems, photoisomerization of azobenzene (Az) is the most favorably incorporated into PDLC devices.

However, understanding the structure and processes of the photoresponsive PDLC in terms of molecular orientation and phase separation behavior is an extremely difficult task in three-dimensional (3D) systems. It is anticipated that lowering the dimensionality from 3D to 2D would offer helpful implications for the structure and photoresponsive mechanism at the molecular level. For the construction of 2D polymer systems, the Langmuir−Blodgett (LB) technique is a powerful tool. Recently, Duran et al. have represented the first examples of a 2D PDLC composed of poly(pentadecylaniline) and a ferroelectric LC (10PPB2) prepared by the LB technique.[14] They have shown that confinement of surfactant molecules to a 2D planar air−water interface allows for the study of complex processes that may otherwise be difficult to observe in the 3D systems.

In these contexts, we conducted a study on preparing a mixed monolayer composed of a photoresponsive polymer and LC via the LB technique. In this approach, poly(vinyl alcohol) (PVA) derivatives having the Az side chain (6Az10-PVA) and 4′-*n*-pentyl-4-cyanobiphenyl (5CB) were used as the amphiphilic Az polymer and LC components, respectively (Figure 1). 5CB was chosen here because the cyano group in the LC molecule works as the hydrophilic head for monolayer formation at the air−water interface.[15−17]

The first part of this paper describes the compatibility between the polymer and the LC at the monolayer level on the water surface. In particular, we focus on the conditions of phase separation of the two components, using $\pi-A$ isotherms. In the second part, the 2D phase separation is visualized by topological atomic force microscopy (AFM). Finally, the photocontrol of phase separation is achieved via direct photoirradiation of the 2D PDLC film.

2. Experimental Section

Materials. The amphiphilic Az polymer, 6Az10-PVA ($x = 0.26$), was synthesized as described in the literature.[18] The nematic LC molecule, 5CB, was purchased from Dainippon Ink

* Author to whom correspondence should be addressed. E-mail: tseki@apchem.nagoya-u.ac.jp. Tel. and Fax: +81-52-789-4668.
[†] Frontier Research System.
[‡] Tokyo University of Science.
[§] Nagoya University.

10.1021/jp0352534 CCC: $25.00
Published on Web 11/19/2003

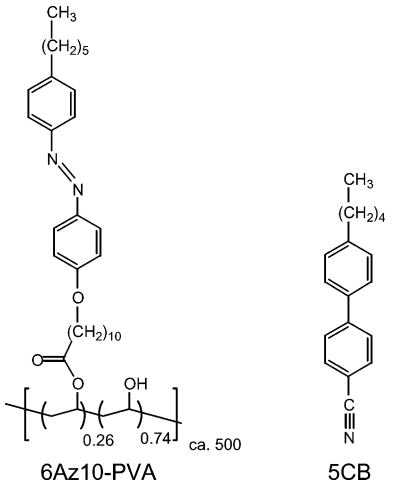

Figure 1. Chemical structures of the materials used.

and Chemicals, Inc., and was used without further purification. The chemical structures of these materials are described in Figure 1. Ultrapure water used for the LB experiments was of Millipore grade (18 MΩ cm^{-1}). Chloroform for monolayer preparation was of spectroscopic grade (Uvasol, Cica-Merck). Mica for the AFM measurements was clear, of slightly stained (C&SS) grade, and purchased from Watanabe Shoko Co.

Monolayer Preparation. The spreading behavior of monolayers at the air−water interface was evaluated on ultrapure water filled in a Lauda FW-1 film balance. The subphase temperature was set at 20 °C using a water circulator (CTE-22W, Komatsu Electronics, Inc.) and controlled within ±0.5 °C. 6Az10-PVA and 5CB were separately dissolved in chloroform at concentrations of 1×10^{-3} and 3×10^{-3} mol dm^{-3}, respectively. Mixed solutions were prepared from these mother solutions at target molar ratios, r = [5CB]/[Az unit]. The solution was spread on ultrapure water, and solvent was allowed to evaporate for approximately 10 min. The monolayer was compressed at a speed of 250 mm^2 min^{-1}, and the surface pressure was monitored.

The single-layer deposition of the monolayer was undertaken in the upstroke onto a freshly cleaved mica fixed on a cleaned quartz plate and a hydrophilic quartz plate washed with a saturated potassium hydroxide/ethanol solution and ultrapure water for AFM and UV−visible (vis) absorption spectroscopy, respectively. Transfer was performed at 2 mN m^{-1} by standard vertical deposition with the dipping speed of 5 mm min^{-1}. All measured values of the transfer ratio were equal to 1.0 ± 0.1, indicating that the monolayer was successfully transferred onto the substrate. Once the transfer was completed, samples were dried in a desiccator overnight.

Physical Measurements. The AFM image was taken using the Seiko Instruments SPA300/SPI3700 in the cyclic contact mode (dynamic force mode) equipped with a 20-μm piezoelectric scanner. A microcantilever of SI-DF20 (rectangular-shaped Si tip) with a force constant of 16.0 N m^{-1} was used. Samples were mounted onto an impact stage that can enable us to slide the samples freely and scanned in at least three different places in a scan area of 5×5 μm^2 to confirm the uniformity of the film morphology.

The film thickness of multilayered LB films was measured by the use of surface profilometry using a Dektak3ST.

UV−vis absorption spectra were recorded on a weak absorption spectrometer (JASCO, MAC-1) at normal incidence in ambient atmosphere. All procedures were carried out in dimmed red light.

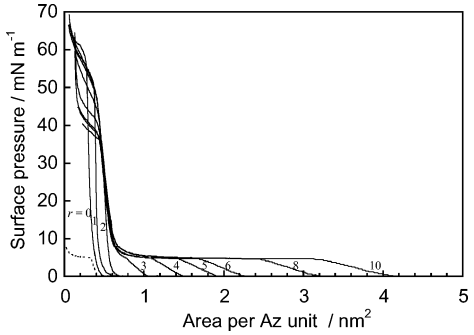

Figure 2. Surface pressure−area isotherms of pure 5CB (broken line, the horizontal axis is expressed as the area per 5CB molecule in this case) and 6Az10-PVA/5CB mixture (solid line) at 20 °C. The numerals in the figure indicate molar ratios (r = [5CB]/[Az unit]).

Photoirradiation. Sample films were irradiated with 365-nm (UV) or 436-nm (vis) light from a Hg−Xe lamp (SAN-EI Electronics, SUPER-CURE 203S) through a combination of glass filters (Toshiba, UV35 + UVD36B, Y43 + V44). The intensity of the light was measured with an ADVANTEST optical power meter (TQ8210) equipped with a photosensor (TQ821017).

3. Results and Discussion

3.1. Monolayer Characterization at the Air−Water Interface. We started with examinations of the spreading behavior of monolayers on the water surface at various mixing ratios. Figure 2 shows $\pi-A$ isotherms of monolayers consisting of a mixture of 6Az10-PVA and 5CB at various molar ratios (r = [5CB]/[Az unit]). The $\pi-A$ isotherms at lower molar ratios (r = 1 and 2) were similar to those of the pure 6Az10-PVA monolayer (r = 0) and showed a slight expansion in the limiting area by 0.08 and 0.23 nm^2, respectively. The increment of the occupying area was, nevertheless, significantly smaller than that anticipated from the pure 5CB monolayer (approximately 0.33 nm^2, as indicated by the broken line). These findings indicate that 5CB is squeezed out partly toward the air side of the monolayer, or these mixed films are composed of a molecular mixture of 6Az10-PVA and 5CB. In any case, the spreading behavior eliminates the possibility of lateral phase separation of the two components.

At higher molar ratios (r > 2), the mixed monolayers exhibited $\pi-A$ isotherms, which could be regarded as the sum of the isotherms of pure 5CB and 6Az10-PVA monolayers. They exhibited an initial collapse at a low pressure (approximately 5 mN m^{-1}) followed by a plateau at this pressure and a final collapse at a high pressure. The collapse at low pressure corresponds to that of the pure 5CB monolayer. Those curves are analogous to the behavior of the separately spread equimolar 6Az10-PVA/5CB monolayer, which forms the heterogeneous and phase-separated structure at the millimeter level.[19] In this range, the increase of r caused the expansion of the plateau region, whereas the limiting area remained constant at 0.62−0.65 nm^2. These features are clearly indicated in Figure 3.

Figure 3 depicts the pressure lift-off area (○), where the pressure rises, and the limiting area (●) estimated from the extrapolation of the steepest region to zero pressure as a function of r, described in the upper part of this figure. A plot of the first lift-off area against r is found to be linear with an inflection at r = 2. The value of 0.43 nm^2 per 5CB molecule estimated from the slope at higher molar ratios (r > 2) is in agreement with the pressure lift-off area of pure 5CB (0.42 nm^2). This good coincidence is strongly indicative of the coexistence of a

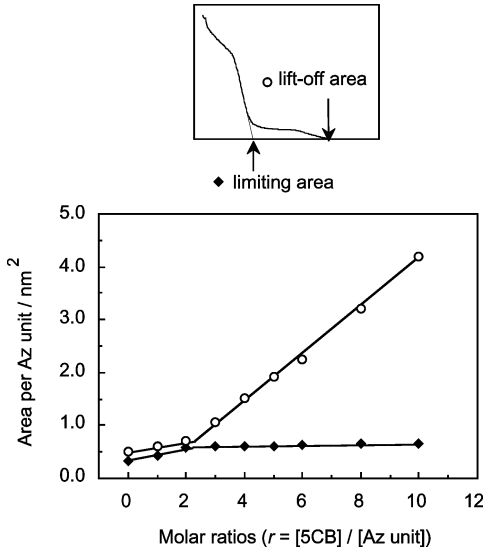

Figure 3. Limiting area (diamonds) and pressure lift-off area (circles) estimated from $\pi-A$ isotherms as a function of r.

pure 5CB monolayer and a mixed monolayer at a low surface pressure ($\pi < 5$ mN m^{-1}) and high molar ratio ($r > 2$). This explanation can account for the fact that the limiting area remained constant because the pure 5CB monolayer collapses and forms a multilayered structure at a high surface pressure ($\pi > 5$ mN m^{-1}).[19]

In summary, the data of $\pi-A$ isotherms support the interpretation that 6Az10-PVA can accommodate two 5CB molecules per Az side chain unit without lateral phase separation. Above this critical ratio, excess 5CB molecules are excluded from the hybrid monolayer and form a phase-separated structure.

3.2. Observation of the Phase Separation Structure by AFM. The 6Az10-PVA/5CB mixed monolayers were observed using Brewster angle microscopy (BAM). BAM is a promising method that allows direct morphological visualization of molecular films at the air−water interface.[20,21] The BAM images taken during the compression process showed differences in the morphologies between the films with the lower ($r < 2$) and higher ($r > 2$) molar ratios. The films with smaller r exhibited a highly homogeneous BAM image up to a high collapse pressure. On the other hand, the morphology of the high-molar-ratio film in the plateau region was characterized by the coexistence of homogeneous parts and patches due to the collapse of the 5CB monolayer. However, monolayers with high molar ratios showed no morphological features at low pressures. This is ascribed to the scale of phase separation being below the resolution limit of BAM. Therefore, the mixed monolayers were observed by AFM.

Transfer of the 6Az10-PVA/5CB mixed monolayers at $r > 2$ was achieved at 2 mN m^{-1} because the random collapse of the monolayer was observed over a wide range when the film of 6Az10-PVA/5CB ($r = 4$) was deposited with further compression above the plateau region. Except for the molecularly mixed monolayer ($r < 2$), the deposition of mixed monolayers was attained at good transfer ratios under this condition.

Topographical AFM images were obtained for each mixture composition ($r = 10$, 8, 6, and 4), as shown in Figure 4. All images clearly show the phase separation of the two components. Circular domains with diameters ranging from 100 to 300 nm were observed within a continuous phase at high molar ratios ($r = 10$, a). As the mole fraction of 5CB decreased, the area of thinner parts decreased, and a number of large distorted domains were observed, seemingly resulting from the coalescence of smaller circular domains. At $r = 4$, the thicker and the thinner parts formed a reticular bicontinuous structure. Taking into account the $\pi-A$ isotherm data, this strongly suggests that the projecting thicker domains are composed of the 6Az10-PVA/5CB molecular hybrid surrounded by the pure 5CB continuous phase.

To investigate the morphological features of the domains, height distribution histograms were taken. Figure 5 shows a typical example. As can be seen from the histogram, the height distribution is not continuous but is comprised of two major contributions. Here, attention was paid to both the area ratio of the two peaks and the height difference (Δh) between the two peaks. The results are presented in Figure 6.

Figure 6a shows the height difference (Δh) between the thicker and the thinner parts as a function of molar ratios ($r =$ [5CB]/[Az unit]). The area corresponding to the hybrid was thicker than that corresponding to the pure 5CB phase by approximately 1.5 nm. This value essentially remained constant in all cases, suggesting that the composition of the hybrid is constant irrespective of the mixing ratio. The absolute thickness of the 6Az10-PVA/5CB hybrid and pure LC layer cannot easily be determined directly from AFM in the cyclic contact mode. The AFM measurements obtained in the contact mode after scratching the film should provide the absolute thickness; however, such a procedure could not be applied to these soft and fragile films. Instead, we assume the absolute thickness as follows. Surface profilometry provided the film thickness of multilayered LB films of the hybrid material. Division of the thickness by the number of layers gave a value of 2.9 nm per monolayer. The thickness of the 5CB monolayer was estimated to be 1.3 nm from the length of the 5CB molecule (1.8 nm)[22] and the average tilt angle of 45° obtained from UV−vis absorption spectra of the 5CB monolayer on the water surface.[23] Subtraction of these values gives a figure of 1.6 nm, which shows outstanding agreement with the experimental value of 1.5 nm.

Figure 6b indicates the ratio of the area of thinner parts to that of thicker parts, R_A, as a function of the molar ratio ($r =$ [5CB]/[Az unit]). Here, the phase separation behavior is analyzed using

$$R_A = B(r - A) \tag{1}$$

where R_A, denotes the area ratio of the thinner part relative to the thicker part and A and B are constants. The solid curve shows the fitted line of this equation.

Equation 1 is based on the following two assumptions. (i) Projecting domains are composed of the 6Az10-PVA/5CB hybrid monolayer. In this hybrid monolayer, the [5CB]/[Az unit] molar ratio is constant (A, corresponding to the intercept with the horizontal axis) in the molar ratio region where phase separation occurs. (ii) The other thinner parts are composed of the pure 5CB monolayer. The ratio of the occupied areas of the pure 5CB monolayer and the hybrid monolayer per Az unit is constant (B, corresponding to the slope). Curve fitting based on AFM data provided the values of A and B of 2.2 and 0.61, respectively. These values can also be obtained from the data on the occupied area at 2 mN m^{-1} as a function of r and are similar to the plot of the lift-off area shown in Figure 3. In the $\pi-A$ isotherms, the occupied area versus r seems to follow two linear regimes with a break at $r = 2.3$. The ratio of the occupied areas of the pure 5CB monolayer (0.38 nm^2) and the hybrid monolayer per Az unit (0.61 nm^2) is calculated to be 0.62. The coincidence between these results is satisfactory and indicates

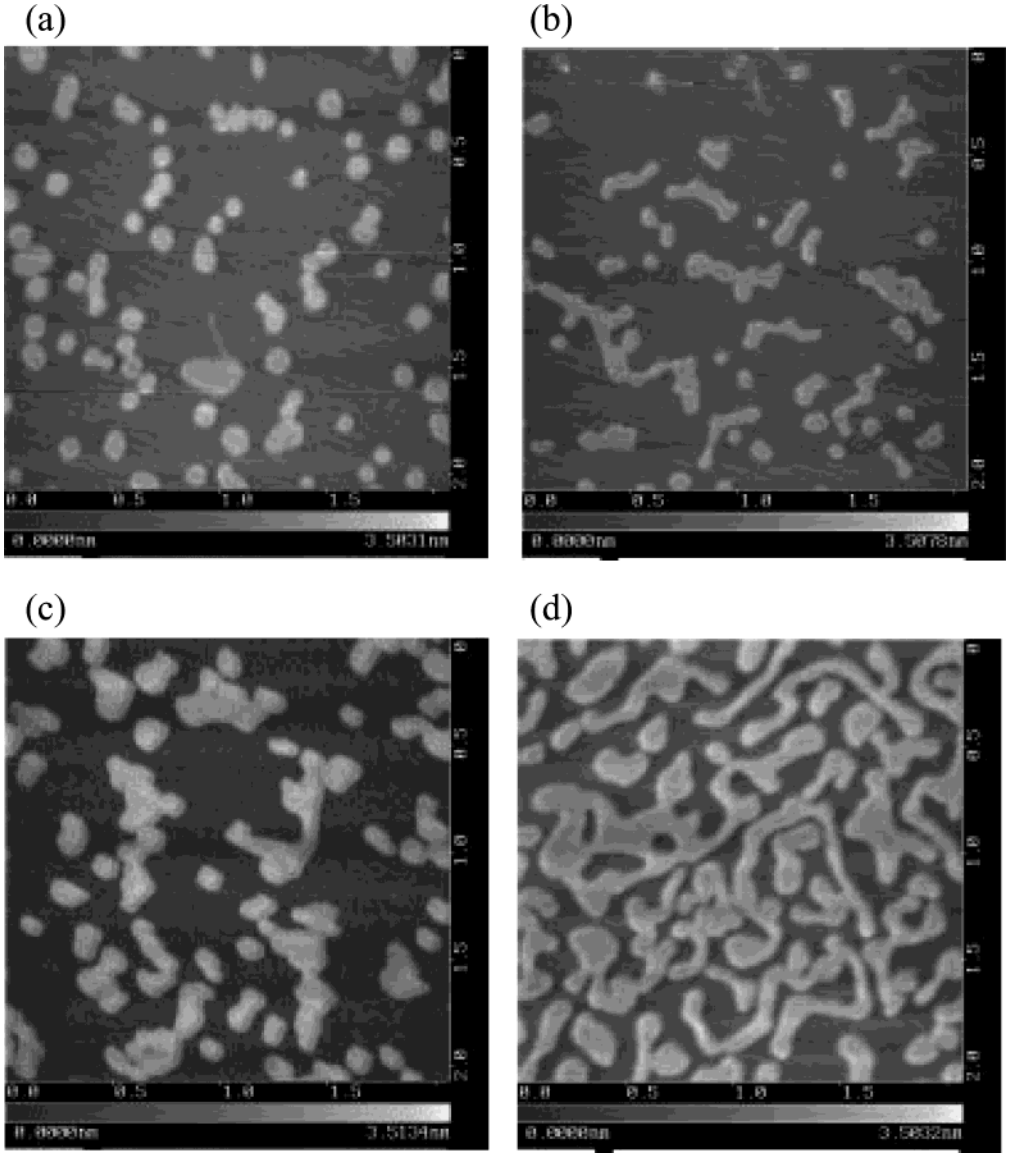

Figure 4. Topographical AFM images of the monolayer consisting of mixtures of 6Az10-PVA/5CB on mica at various molar ratios [$r = 10$ (a), 8 (b), 6 (c), and 4 (d)].

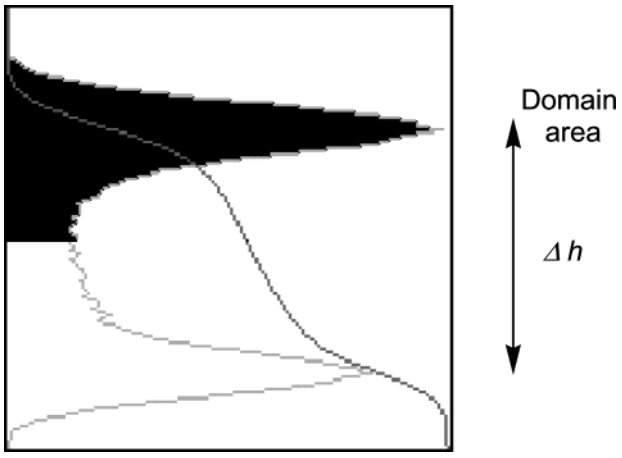

Figure 5. Method for analysis of the AFM image. Representative height profile from the AFM image and its distribution histogram.

that the previous assumptions are reasonable. It is, thus, suggested that phase separation occurs immediately upon the spreading of the film at $r > 2.3$, resulting in a solution-induced phase separation of the hybrid mixture and the pure LC.

The reason for the capacity to accommodate two 5CB molecules with one Az unit is considered as follows. One 5CB molecule can be inserted into the spatial cavity formed between the Az unit and the backbone (spacer part), and the other can be positioned on the air side of the 6Az10 side chain (tail part). In situ X-ray reflectometry showed that the 6Az10-PVA/5CB hybrid monolayer ($r = 1$) was composed of a dense lower layer and a less dense upper layer, indicating that 5CB molecules were inserted into the spatial cavity of the C_{10} spacer part.[24] The fact that homologous Az polymers, having a shorter spacer of C_1 (6Az1-PVA) and C_5 (6Az5-PVA), can accommodate a 5CB molecule up to $r = 1$ without the generation of phase separation supports the latter case.[19]

In summary, the data of AFM as well as $\pi-A$ isotherms support the following scenarios. 6Az10-PVA and 5CB molecules are compatible at a molecular level at lower molar ratios ($r < 2$). At higher molar ratios ($r > 3$), on the other hand, excess 5CB molecules are excluded from the hybrid monolayer and start to undergo lateral phase separation at the submicrometer scale.

3.3. Photoresponsive Behavior. To observe the photoresponsive behavior of the monolayer, spectral measurements were

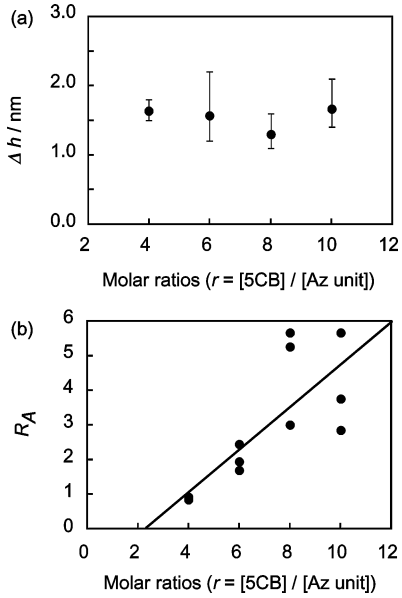

Figure 6. Data analysis of the AFM images. (a) Average difference of the thickness of the phase-separated monolayer as a function of *r*. (b) Area ratio of the thinner part relative to thicker part, R_A, as a function of *r*.

carried out. Figure 7 shows UV−vis absorption spectra of the monolayer of 6Az10-PVA/5CB at $r = 4$ deposited on both sides of a quartz substrate. The film was first irradiated with 365-nm (UV) light (a) followed immediately by 436-nm (vis) light (b). The solid curves show the two spectra of the film before and after irradiation to the photoequilibrated state.

In the initial trans state of Az, the long-axis $\pi-\pi^*$ band for Az was notably small, indicating perpendicular orientation to the substrate plane. Also, the spectral peak was positioned at approximately 350 nm, which shows that the Az unit exists in the nonaggregated state. These features are analogous to those of the equimolar hybrid monolayer.[19] On the other hand, the long-axis $\pi-\pi^*$ band of cyanobiphenyl at 280 nm was considerably larger than that of the equimolar hybrid monolayer, taking into account the differences of the mixing ratios and occupied areas. It is thought that the 5CB molecules excluded from the hybrid monolayer adopt a more random orientation than the homeotropic one in the hybrid part.

The features of the spectral changes were essentially the same as those of the equimolar mixed monolayer described in our previous report.[19] Irradiation with UV light increased the absorption intensity of the $n-\pi^*$ transition peaking around 440 nm. This unequivocally indicates the progress of the trans-to-cis photoisomerization of Az. Concomitantly, a large absorption enhancement in the band region of 280 nm was observed. Because normal incidence was adopted in these experiments, the spectral changes can be ascribed to the induction of the orientational change of the 5CB molecule from the perpendicular to a tilted state. The enhancement of the absorption band at 280 nm was approximately synchronized with that of the $n-\pi^*$ band of Az. This indicates that the orientational changes of 5CB are induced by the photoisomerization of the Az side chain. The reverse process could also be induced by vis light irradiation (Figure 7b). The enhanced absorption band around 280 nm reverted to almost the original level upon irradiation.

A different phenomenon was observed for the phase-separated monolayer compared to the behavior of the equimolar hybrid monolayer; the absorption intensity around 600 nm showed a temporary enhancement, which was a temporal decrease in the transmittance, in the process of irradiation with both UV and vis light, as shown by the broken line in Figure 7. From the change in the region of 400−500 nm ($n-\pi^*$), photoequilibration was achieved within an exposure energy of 0.4 J cm^{-2}, which was only a few times larger than that in solution, in both processes of the trans-to-cis and cis-to-trans photoisomerization. In contrast, further exposure (0.7 J cm^{-2} and 3.6 J cm^{-2} upon UV and vis light irradiation, respectively) was required to cause suppression of the decrease in transmittance around 600 nm as well as the complete orientational change of 5CB molecules.

Because no chromophores that absorb light in these wavelength regions exist, we have to consider another reason for the apparent decrease in transmittance. Further discussion will be described after the explanation for Figure 8.

Figure 8 shows changes in topographical AFM images of the monolayer of 6Az10-PVA/5CB at $r = 4$ deposited on a mica substrate after dark adaptation for a week in dry atmosphere (Figure 8a). The film was first irradiated with UV light and then with vis light under highly humid conditions (relative humidity of approximately 95%).

After UV light irradiation (2.4 J cm^{-2}), virtually all domains disappeared, resulting in smoother film with a surface roughness within 0.2 nm (Figure 8b). Subsequent vis light irradiation (2.4 J cm^{-2}) regenerated the thicker domains of 50−100 nm in diameter and approximately 1.5 nm in height (Figure 8c). Although the size of each projected domain became smaller, phase separation occurred again. The precise estimation of the height difference and coverage of the domain in the manner presented in Figure 5 was difficult because the height distribution histogram showed only one broadened peak. Nevertheless, the round domains were thicker than the thinner regions by 1.5 nm, indicating a good coincidence with those of the initial state before photoirradiation.

These results could be explained on the basis of a photochemical phase transition.[25,26] The trans-to-cis isomerization of Az induced by UV light made a thick spin-cast hybrid film isotropic phase starting from the LC phase composed of trans Az and LCs. This change also induced the film softening. In fact, when the film was irradiated with UV light through a photomask, all the irradiated regions were readily scratched by the tip of the surface profilometer.

Taking account of such results obtained with thicker films, we can consider the phenomena occurring in the monolayer state. When the phase-separated monolayer was exposed to UV light, the hybrid would mingle with the excess 5CB molecules as a result of higher molecular diffusions in the fluid isotropic phase, which then would lead to the formation of a flat surface. In the reverse process of cis-to-trans isomerization, a hybrid complex composed of one Az side chain and two 5CB molecules should be formed, and then, the phase separation would occur again, repelling the excess 5CB molecules. The 2D diffusion of molecules can be supported by the fact that more regularly dispersed phase-separated domains were observed after the back process, as shown in Figure 8c.

It was also confirmed by AFM observation that the flat film was considerably softened. The tapping procedure by the AFM tip inscribed the flat softened surface and increased the surface roughness from 0.2 to 0.6 nm. In this experiment, it was also suggested that the film in the photostationary cis-rich state in the dark is not fully liquidlike but is probably in a somewhat plasticized state because the rough surface morphology was maintained for a prolonged duration. This is somewhat contradictory to the fact that the molecularly flat surface is spontaneously obtained after UV irradiation. One explanation for this would be that the film becomes highly fluid only during

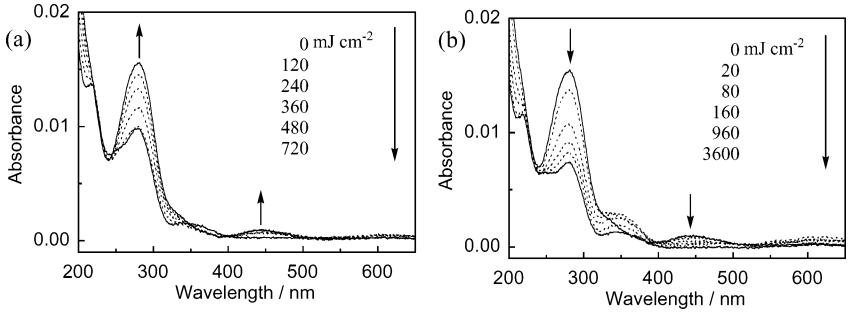

Figure 7. UV−vis spectral changes of the 6Az10-PVA/5CB mixed monolayer ($r = 4$) on both sides of a quartz substrate transferred at 2 mN m^{-1} upon exposure to UV (365 nm, a) and subsequent vis (436 nm, b) light.

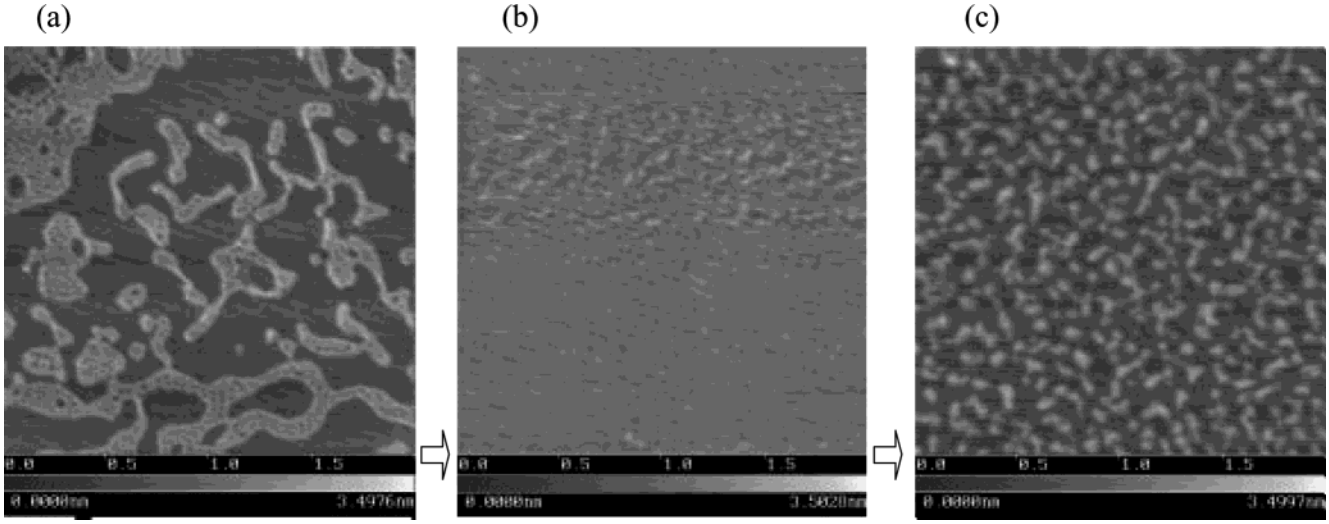

Figure 8. Topographical AFM images of the 6Az10-PVA/5CB mixed monolayer ($r = 4$) before photoirradiation (a), after UV light irradiation (b), and after subsequent vis light irradiation (c) at a high humidity (approximately 95%).

photoirradiation, where Az units are in a "hot" state that provides local heat and active geometrical alternation between the cis/trans isomers.[27]

The marked morphological changes were promoted under highly humid conditions. However, essentially no morphological changes were observed under dry atmospheric conditions (approximately 30%) with irradiation of UV light at 1.0 J cm^{-2}. The humidity dependence observed here undoubtedly shows that the hydration of monolayers on mica[28] plays a critical role in providing the dynamic nature of the film material.[29]

The temporal decrease in the transmittance around 600 nm in Figure 7 can be ascribed to the morphological change shown in Figure 8. We assume that the temporal decrease in the transmittance should be attributed to the scattering of light resulted from the formation of microscopic structures in the 2D phase separation. Actually, Menzel reported the light scattering due to phase separation induced by light in the multilayered LB films composed of photoisomerizabale low-molecular-weight dye and hairy-rod polymer, though the phase-separated crystalline size is up to 20 μm in diameter.[30] In any event, the phase separation state can be controlled by the photoisomerization of Az, and our AFM data provides the direct evidence for this.

The photoinduced fluidity change between the trans and the cis forms also plays an important role in the striking improvement of the surface relief formation efficiency in a 6Az10-PVA/5CB hybrid spin-cast film.[31] In such systems, the material transfer efficiency is markedly enhanced by more than 2 orders of magnitude in the softened films. Film softening was attained by the combination of the addition of a LC into the film as a plasticizer and the pre-UV light irradiation to generate the cis Az form in this system. The exceedingly rapid photoinduced mass migration was attained along with stiffening of the hybrid film as a result of the back isomerization of Az to the trans form by the argon ion laser that corresponded to the vis light. The stoichiometric ratio ($r = 2$) observed in the 2D molecular film was coincident with the most efficient condition for photoinduced surface relief formation and the compatible criterion as revealed in the bulk state using differential scanning calorimetry.[31] It was shown that the criterion between compatibility and phase separation of the 2D molecular film corresponded with that of the 3D film (100-nm thickness) and bulk.

4. Conclusion

Langmuir films composed of mixtures of a hydrophilic PVA having a hydrophobic Az side chain (6Az10-PVA) and a nematic LC, 5CB, were prepared at various molar ratios (r = [5CB]/[Az unit]). Surface pressure−area isotherms, visualization by BAM, and UV−vis absorption spectroscopy revealed that the two components were homogeneously mixed at a molecular level and form a hybrid monolayer up to $r = 2$. Under 5CB-rich conditions at $r > 2$, phase separation started to occur. The mixed monolayers were then transferred onto a mica substrate by the LB method. Images of AFM showed that submicrometer-scale lateral phase separation occurred when $r > 2$. These results imply that 6Az10-PVA can accommodate two 5CB molecules per Az side chain without phase separation and that, above this ratio, lateral phase separation involving the projecting hybrid monolayer and the pure 5CB monolayer starts to occur. It was

further observed that the photochemical control of the phase separation was possible with alternating irradiation of UV and vis light.

The results described in this paper clearly show the versatility and validity of the 2D system for the observation and understanding of the phase separation behavior and its photoresponse. The data obtained here will provide useful information on the 3D PDLC systems. It is indicated here, although very preliminarily, that the light scattering modulation at around 600 nm is actually induced by the photoprocess.

Acknowledgment. We thank Drs. S. Morino, M. Nakagawa, and K. Arimitsu in our laboratory for technical assistance and discussions. This work was in part supported by the Grant-in-Aid for Scientific Research on the Priority Areas (417) from the Ministry of Education, Culture, Sports, Science and Technology, and the CREST Program of Japan Science and Technology Corporation.

References and Notes

(1) Kato, T. *Science* **2002**, *295*, 2414.
(2) Kajiyama, T.; Miyamoto, A.; Kikuchi, H.; Morimura, Y. *Chem. Lett.* **1989**, 813.
(3) Crawford, G. P., Zumer, S., Eds.; *Liquid Crystals in Complex Geometries; Formed by Polymer and Porous Networks*; Taylor & Francis: London, 1996; Vol. 1, p 1.
(4) Montgomery, G. P., Jr.; Smith, G. W.; Vaz, N. A. In *Liquid Crystalline and Mesomorphic Polymers*; Shibaev, V. P., Lam, L., Eds.; Springer: Heidelberg, 1994; Vol. 5, p 149.
(5) Fergason, J. L. *SID Dig. Tech. Pap.* **1985**, 68.
(6) Doane, J. W.; Vaz, N. A.; Wu, B.-G.; Zumer, S. *Appl. Phys. Lett.* **1986**, *48*, 269.
(7) Yang, D.-K.; Doane, J. W. *SID Dig. Tech. Pap.* **1992**, 759.
(8) Kikuchi, H.; Yokota, M.; Hisakado, Y.; Yang, H.; Kajiyama, T. *Nat. Mater.* **2002**, *1*, 64.
(9) Balkanski, M.; Lallemand, P. *Photonics*; Gauthier-Villars: Montreal, 1975.
(10) Kawanishi, Y.; Tamaki, T.; Ichimura, K. *Appl. Phys. D* **1991**, *24*, 782.
(11) Lee, H.-K.; Kanazawa, A.; Shiono, T.; Ikeda, T. *Chem. Mater.* **1997**, *10*, 11402.
(12) Kurihara, S.; Matsumoto, K.; Nonaka, T. *Appl. Phys. Lett.* **1998**, *73*, 160.
(13) Morino, S.; Kaiho, A.; Ichimura, K. *Appl. Phys. Lett.* **1998**, *73*, 1317.
(14) (a) Herod, T. E.; Duran, R. S. *Langmuir* **1998**, *14*, 6606. (b) Kloeppner, L. J.; Duran, R. S. *Langmuir* **1998**, *14*, 6734. (c) Herod, T. E.; Duran, R. S. *Langmuir* **1998**, *14*, 6956.
(15) Xue, J.; Jung, C. S.; Kim, M. W. *Phys. Rev. Lett.* **1992**, *69*, 474.
(16) Friedenberg, M. C.; Fuller, G. G.; Frank, C. S.; Robertson, C. R. *Langmuir* **1994**, *10*, 1251.
(17) de Mul, M. N. G.; Mann, J. A., Jr. *Langmuir* **1994**, *10*, 2311.
(18) Seki, T.; Sakuragi, M.; Kawanishi, Y.; Suzuki, Y.; Tamaki, T.; Fukuda, R.; Ichimura, K. *Langmuir* **1993**, *9*, 211.
(19) (a) Ubukata, T.; Morino, S.; Seki, T.; Ichimura, K. *Chem. Lett.* **1998**, 71. (b) Ubukata, T.; Seki, T.; Ichimura, K. *J. Phys. Chem. B* **2000**, *104*, 4141.
(20) Hénon, S.; Meunier, J. *Rev. Sci. Instrum.* **1991**, *62*, 936.
(21) Hönig, D.; Möbius, D. *J. Phys. Chem.* **1991**, *95*, 4590.
(22) Smith, D. P. E.; Hörber, H.; Gerber, Ch.; Binnig, G. *Science* **1989**, *245*, 43.
(23) Ubukata, T. Master Thesis, Tokyo Institute of Technology, Tokyo, Japan, 1998.
(24) Kago, K.; Seki, T.; Schucke, R. R.; Mouri, E.; Matsuoka, H; Yamaoka, H. *Langmuir* **2002**, *18*, 3875.
(25) Pelzel, G. *Z. Chem.* **1977**, *17*, 294.
(26) (a) Ikeda, T.; Tsutsumi, O. *Science* **1995**, *268*, 1873. (b) Sung, J. H.; Hirano, S.; Tsutsumi, O.; Kanazawa, A.; Shiono, T.; Ikeda, T. *Chem. Mater.* **2002**, *14*, 385. (c) Ikeda, T.; Kanazawa, A. *Bull. Chem. Soc. Jpn.* **2000**, *73*, 1715.
(27) Srikhirin, T.; Laschitsch, A.; Neher, D.; Johannsmann, D. *Appl. Phys. Lett.* **2000**, *77*, 963.
(28) Beaglehole, D.; Radlinska, E. Z.; Ninham, B. W.; Christenson, H. K. *Phys. Rev. Lett.* **1991**, *66*, 2084.
(29) (a) Seki, T.; Tanaka, K.; Ichimura, K. *Macromolecules* **1997**, *30*, 6401. (b) Seki, T.; Kojima, J.; Ichimura, K. *Macromolecules* **2000**, *33*, 2709.
(30) Menzel, H. *Macromolecules* **1993**, *26*, 6226.
(31) (a) Ubukata, T.; Seki, T.; Ichimura, K. *Adv. Mater.* **2000**, *12*, 1675. (b) Ubukata, T.; Seki, T.; Ichimura, K. *Colloids Surf., A* **2002**, *198*, 113.